

Enhanced Photosensitization by Carbon Dots Co-adsorbing with Dye on p-Type Semiconductor (Nickel Oxide) Solar Cells

Habtamu Fekadu Etefa, Toyoko Imae,* and Masatoshi Yanagida

Cite This: *ACS Appl. Mater. Interfaces* 2020, 12, 18596–18608

Read Online

ACCESS |



Metrics & More



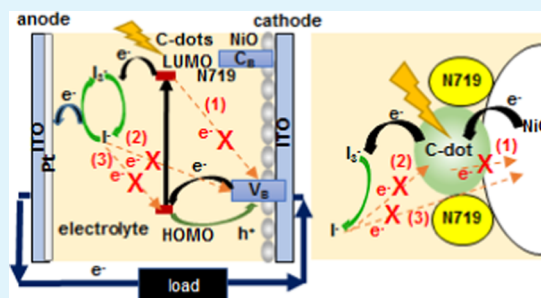
Article Recommendations



Supporting Information

ABSTRACT: In this work, the effect of carbon dots (C-dots) on the performance of NiO-based dye-sensitized solar cells (DSSCs) was explored. NiO nanoparticles (NPs) with a rectangular shape (average size: 11.4×16.5 nm²) were mixed with C-dots, which were synthesized from citric acid (CA) and ethylenediamine (EDA). A photocathode consisting of a composite of C-dots with NiO NPs (NiO@C-dots) was then used to measure the photovoltaic performance of a DSSC. A power conversion efficiency (PCE) of 9.85% (430 nm LED@50 mW/cm²) was achieved by a DSSC fabricated via the adsorption of N719 sensitizer with a C-dot content of 12.5 wt % at a 1.5:1 EDA/CA molar ratio. This PCE value was far larger than the PCE value (2.44 or 0.152%) obtained for a NiO DSSC prepared without the addition of C-dots or N719, respectively, indicating the synergetic effect by the co-adsorption of C-dots and N719. This synergetically higher PCE of the NiO@C-dot-based DSSC was due to the larger amount of sensitizer adsorbed onto the composites with a larger specific surface area and the faster charge transfer in the NiO@C-dot working electrode. In addition, the C-dots bound to the NiO NPs shorten the band gap of the NiO NPs due to energy transfer and give rise to faster charge separation in the electrode. The most important fact is that C-dots are the main sensitizer, while N719 tightly adsorbs on C-dots and NiO behaves as an accelerator of a positive electron transfer and a restrainer of the electron–hole recombination. These results reveal that C-dots are a remarkable enhancer for NiO NPs in DSSCs and that NiO@C-dots are promising photovoltaic electrode materials for DSSCs.

KEYWORDS: nickel oxide, carbon dot, nickel oxide@carbon dots composite, power conversion efficiency, dye-sensitized solar cell



1. INTRODUCTION

Dye-sensitized solar cells (DSSCs), which are one of the most promising types of renewable energy-generating devices, have attracted research interest, as they mainly use photons from sunlight to generate electrical energy from solar energy.^{1,2} Many researchers have actively focused on the performance of DSSCs, which utilize low-cost/low-weight materials and are easily handled.^{3–6} However, compared to that of other classes of solar cells, the efficiency performance of such devices is still low, and thus, many researchers are competing to solve this problem.

Currently, metal oxide nanoparticles (NPs) are inspiring the world because of their potential applications. For instance, NiO NPs have been chosen as alternative electrodes on DSSCs because of their facile and reliable synthesis and characteristic electrical and optical properties since they are well-known p-type transition-metal semiconductors.⁷ This enables excitons to be generated by capturing photons at the electrode in DSSCs. In the last few years, some research works have realized NiO NP-based DSSCs, which have been improved by hybridization with other metal oxides such as TiO₂ and ZnO and reached power conversion efficiency (PCE) values of 3.80 and 3.01%, respectively,^{8,9} although a p-type DSSC using NiO NPs as a working electrode achieved an efficiency of only 1.3%.

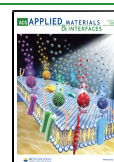
To the best of our knowledge, these results represent the highest efficiency reported for NiO p-type DSSCs to date; thus, the performance of NiO-based DSSCs remains unsatisfactory. Therefore, as the poor performance of NiO-based DSSCs may be due to their low carrier mobilities and charge recombination,¹⁰ there is still a need to enhance/modify the performance of NiO-based DSSCs.

A carbon dot (C-dot) is the smallest outcome (below 5 nm in size) of all carbon allotropes and is known as a zero-dimensional fluorescent carbon analogue, which is highly interesting due to its photoluminescence and prospects for assisting prominent nanoscale size features.^{11,12} Synthesized C-dots thoroughly differ from many kinds of carbon allotropes because they consist of desirable functional groups such as hydroxyl, carboxyl, and amine moieties, which are effective in water dispersibility and result in excellent chemical reactivity.¹³ Thus, C-dots have attracted the attention of researchers as

Received: February 8, 2020

Accepted: April 2, 2020

Published: April 2, 2020



newly emerging carbon substances due to their outstanding biocompatibility,¹⁴ low toxicity,¹⁵ and strong absorption of light, among others, as well as their water dispersibility, and they demonstrate a tremendous potential for applications in various fields.¹⁶

Moreover, metal oxide composites containing C-dots possess potential for many applications, and they are attractive for the achievement of high optical performance (fluorescence emission).¹⁷ Consequently, the addition of C-dots to metal oxides increases their performance.¹⁸ This view shows that C-dots can enhance electron transfer and reduce charge recombination because they serve as an energy donor in electrochemical devices such as supercapacitors and DSSCs.¹⁹ Incidentally, recent work has reported that the PCE of a ZnO DSSC increases from 0.8 to 5.9% following the addition of C-dots.²⁰ This result indicates that the addition of C-dots has an immense potential to increase the efficiency of DSSCs. Thus, we have seen that C-dots are very effective in improving electrochemical performance when they were added to the metal oxide in a DSSC.

In this work, we prepared composites of NiO NPs with C-dots to improve the PCE of NiO NPs in DSSC and to assess the effect of C-dots on a NiO NP DSSC. This objective was achieved by first synthesizing NiO NPs and C-dots. Subsequently, composites of C-dots with NiO NPs were formed under appropriate conditions to optimize the efficiency of composites for use in a DSSC, which was fabricated using two different dyes, di-tetrabutylammonium *cis*-bis-(isothiocyanato)bis(2,2'-bipyridyl-4,4'-dicarboxylato) ruthenium(II) (N719) and rhodamine 6G (Rh6G), as sensitizers. The effects of C-dots with different ratios of component substances and at different C-dot contents in composites were compared. Finally, the effect of C-dots on NiO DSSCs was discussed. Thus, we expect the C-dots to serve as a prospective low-cost additive that enhances the performance of photovoltaic devices.

2. EXPERIMENTAL SECTION

2.1. Reagents. Citric acid anhydrous (CA, 99.5%), nickel chloride (NiCl₂, 98%), Rh6G (99%), ethylenediamine (EDA, 99%), and acetonitrile (99.5%) were purchased from Across Organic. Iodine (I₂, 98%) was a product from Tokyo Chemical Industry (Japan). Sodium hydroxide (99%) and ethyl alcohol (99.5%) were obtained from J. T. Baker (Sweden) and Choneye Pure Chemicals (China), respectively. N719 and indium tin oxide (ITO) glass were purchased from Solaronix (Switzerland) and Aimcore Technology (Taiwan), respectively.

2.2. Synthesis of Composites of C-dots with NiO NPs (NiO@C-Dots). NiO NPs were synthesized using the calcination method.²¹ Nickel hydroxide (Ni(OH)₂) was prepared by dropwise adding 0.4 M NaOH to a 0.2 M nickel chloride solution and by stirring for 1 h at 80 °C under pH 12.7. Precipitates were collected by centrifugation and washed three times with water (25 mL) and once with ethyl alcohol. The wet green cake obtained was air-dried at room temperature for 12 h (overnight) and calcined at 350 °C for 2.5 h. Then, black NiO NPs were obtained.

C-dots were synthesized by the hydrothermal method.²² CA (1 g) was dissolved in water (60 mL), sonicated for 5 min, and added with EDA (174, 300, 520, 694, and 868 μL). The molar ratios of EDA/CA were 0.5:1, 1.0:1, 1.5:1, 2.0:1, and 2.5:1, respectively. The mixture was stirred for 25 min at room temperature, carbonized hydrothermally in an autoclave at 230 °C for 5 h, and then cooled to room temperature. The brown transparent dispersion of C-dots obtained evaporated the solvent using a rotary evaporator, and the obtained brown powder of C-dots was dried in a vacuum oven at 40 °C. The size of carbon dots determined from the transmission electron microscopic images was

2.5 ± 1.5 nm (Supporting Information (SI), Figure S1). According to the X-ray diffraction results, the content ratio of carbon/oxygen increased from 1.14 to 1.28 and that of carbon/nitrogen decreased from 4.00 to 3.00 for C-dots at EDA/CA from 1:1 to 1.5:1.

C-dots (22, 45, 57.5, 71, and 100 mg) at an EDA/CA molar ratio of 1:1 were dispersed in water (2 mL) under 15 min sonication, and separately NiO (400 mg) was dispersed in water (2 mL) and sonicated for 15 min. Then, the two dispersions were mixed and stirred for 4 h. The solid was collected by centrifugation at 6000 rpm, washed once with ethanol and twice with water, and dried in a vacuum oven at 40 °C for 3 h. Then, the calculated contents of C-dots in NiO@C-dots were 5, 10, 12.5, 15, and 20 wt %. Separately, the mixed products of NiO (400 mg) with C-dots (57.5 mg) at various EDA/CA molar ratios were prepared by the same procedure described above. In this case, the content of C-dots in NiO@C-dots was 12.5 wt %.

2.3. Characterization. Transmission electron microscopy (TEM, JEOL, JEM-2000FXII, Japan) was run at a 120 kV accelerated voltage. The specimens were prepared by putting dropwise an aqueous dispersion of NiO and NiO@C-dots on the carbon-covered copper grid and dried. Ultraviolet–visible (UV–vis) absorption spectra (JASCO V-670, Japan) were analyzed using a 1 mm quartz cell at a scan speed of 200 nm/min and the wavelength region of 200–800 nm. Fourier transform infrared (FT-IR) absorption spectra at 400–4000 cm⁻¹ were taken at room temperature using potassium bromide (KBr) pellets on a Nicolet 6700 (Thermo Scientific) with an accumulation of 64 times. The X-ray diffraction system (XRD, Bruker, D2 Phaser, Karlsruhe, Germany) was settled at the 2θ degree of 30–80° using Cu Kα radiation (λ = 1.54 Å) at 40 kV. Nitrogen (N₂) adsorption–desorption isotherms were measured at 77 K on a BELSORB Max, Japan. Before the isotherm measurement, 560 mg of NiO NPs and NiO@C-dots were preheated at 300 °C for 3 h. X-ray photoelectron spectroscopy (XPS, VG Scientific ESCALAB 250, England) measurements were achieved for NiO NPs and NiO@C-dots, which were redried at 40 °C in a vacuum oven.

2.4. Measurements of Photocurrent (*I*–*V*), Electrochemical Impedance Spectra and Incident Monochromatic Photon-to-Current Conversion Efficiency. A transparent semiconducting ITO glass was precleaned once with acetone and twice with water and by UV light irradiation in vacuum for 5 min (H0017, Japan). The dispersions of NiO NPs (100 mg) and NiO@C-dots (100 mg) in water (400 μL) were separately stirred for 4 h. Using a spin coater (K-359SD-1 SPINNER, KYOWA RIKEN, Japan) at 2000 rpm, the aqueous dispersions of NiO NPs and NiO@C-dots were coated on a 1 × 1 cm² area of the precleaned ITO glass and dried. The NiO NPs and NiO@C-dot electrodes annealed in an oven at 350 °C for 25 min were immersed for 12 h in an ethanol solution (5 mL) of N719 (0.5 mM) or Rh6G (5 mM) dyes separately. The NiO NPs and NiO@C-dot photocathode films (0.142 mm thickness) on ITO were assembled with the platinum (Pt)/ITO counter electrode. The redox electrolytes (0.3 M KI, 0.05 M I₂, and 10 mL of acetonitrile solvent) were filled between two assembled film electrodes on ITO. The *I*–*V* measurement was carried out using ZAHNER, Xpot, 26356, Germany, using a light source of blue (430 nm)-light-emitting diode (LED). The calculation of total PCE (η) at the intensity of the light incident (*P*_{in} = 50 mW/cm²) follows the equation below.

$$\eta = \frac{J_{sc} V_{oc}}{P_{in} FF} \quad (1)$$

where *J*_{sc} is the short-circuit current density, *V*_{oc} is the open-circuit voltage, and FF is the fill factor.

Electrochemical impedance spectra (EIS, Zennium, 40442, German) were measured at a frequency of 1–100 kHz and an amplitude of 10 mV using the three-electrodes system. The film was prepared by mixing 100 μL of Nafion and 900 μL of ethanol (99%), sonicating for 10 min, adding 20 mg of NiO or NiO@C-dots to this solution, sonicating for 2 h separately, and coating them on ITO glass using a spin coater (K-359SD-1, SPINNER KYOWA RIKEN, Japan). The Bode phase plot from EIS was analyzed based on

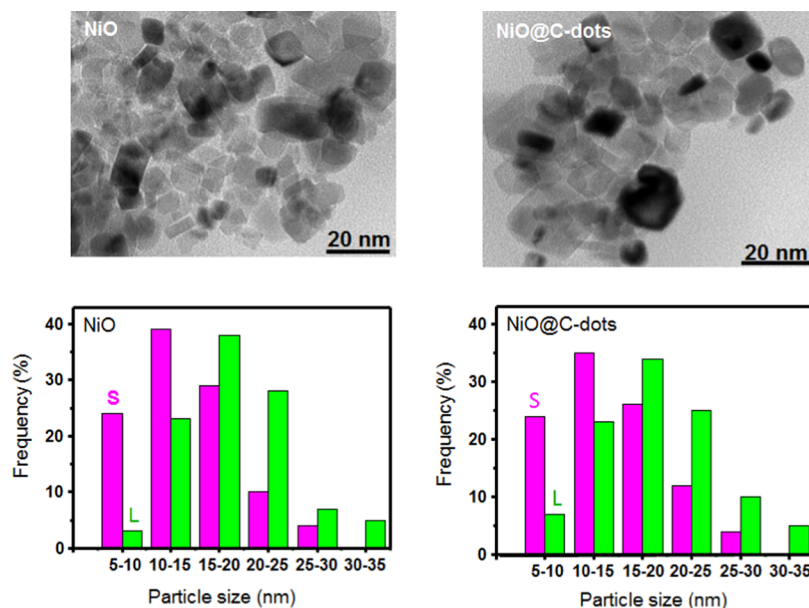


Figure 1. (Top) TEM images and (bottom) size distribution histograms of NiO NPs and NiO@C-dots. S: short axis, L: long axis.

$$\tau_e = \frac{1}{\omega_{\text{mid}}} = \frac{1}{2\pi f_{\text{mid}}} \quad (2)$$

where τ_e is the relaxation time, ω_{mid} is the middle angular frequency, and f_{mid} is the middle frequency of the peak.

The incident monochromatic photon-to-current conversion efficiency (IPCE) was measured on a solar simulator (Wacom WXS 220S-L2, Japan).

2.5. Measurements of Adsorption Amount of Dyes.

Adsorption amounts of N719 and Rh6G on adsorbents (NiO NPs and NiO@C-dots at 12.5 wt % of C-dots) were measured as follows: NiO NPs (1.596 mg) and NiO@C-dots (1.599 mg) coated on the ITO glass ($1 \times 1 \text{ cm}^2$) (see Section 2.4) were annealed in an oven at $350 \text{ }^\circ\text{C}$ for 25 min. The annealed electrodes were immersed in ethanol (5 mL) solutions of N719 (0.5 mM) and Rh6G (5 mM) for 12 h separately. After the extra dyes were washed out using water, the electrodes were immersed in an aqueous 1 M solution (5 mL) of NaOH for 12 h separately to extract dye loaded on the NiO NPs and NiO@C-dots electrodes. The concentrations of the dyes in the extractants were calculated via calibration curves by the calorimetric procedure (UV-vis, JASCO V-670, Japan), where the absorbances of a 310 nm absorption band of N719 and a 380 nm absorption band of Rh6G were utilized.

3. RESULTS AND DISCUSSION

3.1. Characterization of Materials.

NiO NPs were synthesized by the calcination method, and their sizes and shapes were determined by the TEM. The rectangular NiO NP crystals (Figure 1) were confirmed identical to a previously reported structure.²³ The size histogram shown in Figure 1 indicates average particle sizes of short and long axes as well as their respective distributions of 11.37 ± 0.53 and 16.48 ± 0.26 nm, respectively. Figure 1 also shows a TEM image of the NiO NP composite with C-dots. Although similar shape and size of NiO NPs (11.27 ± 0.20 and 16.56 ± 0.32 nm for short and long axes, respectively) are recognizable, C-dots are not distinguished clearly on the NiO NPs and even in the background. These results suggest the unconfirmed existence of C-dots in the TEM image due to the C-dots having a lower X-ray density than NiO NPs.

The FT-IR spectra of C-dots, NiO NPs, and NiO@C-dots are shown in Figure 2A. The major band of NiO NPs that

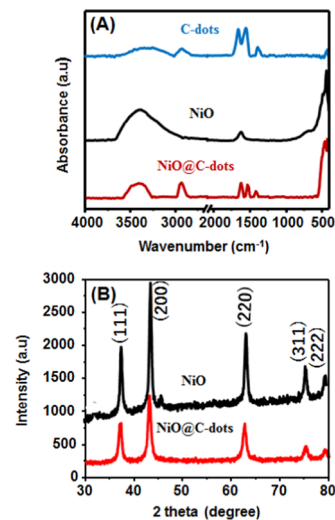


Figure 2. (A) FT-IR absorption spectra of NiO NPs, C-dots, and NiO@C-dots and (B) XRD spectra of NiO NPs and NiO@C-dots.

appeared at 436 cm^{-1} can be assigned to the stretching vibration mode of Ni–O. The bands at 3420 and 1644 cm^{-1} are the contribution of OH stretching and bending modes, which should have come from the hydration or hydroxylation on the NiO NP surface or the water adsorption. Five major bands of C-dots appear at 3390 , 2931 , 1662 , 1557 , and 1390 cm^{-1} and are ascribed to the respective O–H, C–H, C=O, N–H/C=C, and C=C vibration modes of carboxylic acid (O–H, C=O), alkyl (C–H), amine (N–H), and graphitic (C=C) functional groups.¹⁶ However, NiO@C-dots possess characteristic bands of both NiO NPs and C-dots, indicating the coexistence of both components. As a result, the FT-IR spectra suggest that C-dots coexist with NiO NPs.

As revealed in Figure 2B, the XRD peaks and the peak positions are in relatively good agreement with the previously reported cubic phase structure (corresponding to the wurtzite structure) of NiO NPs.²⁴ Correspondingly, all of the indexed diffraction peaks appeared as (111), (200), (220), (311), and

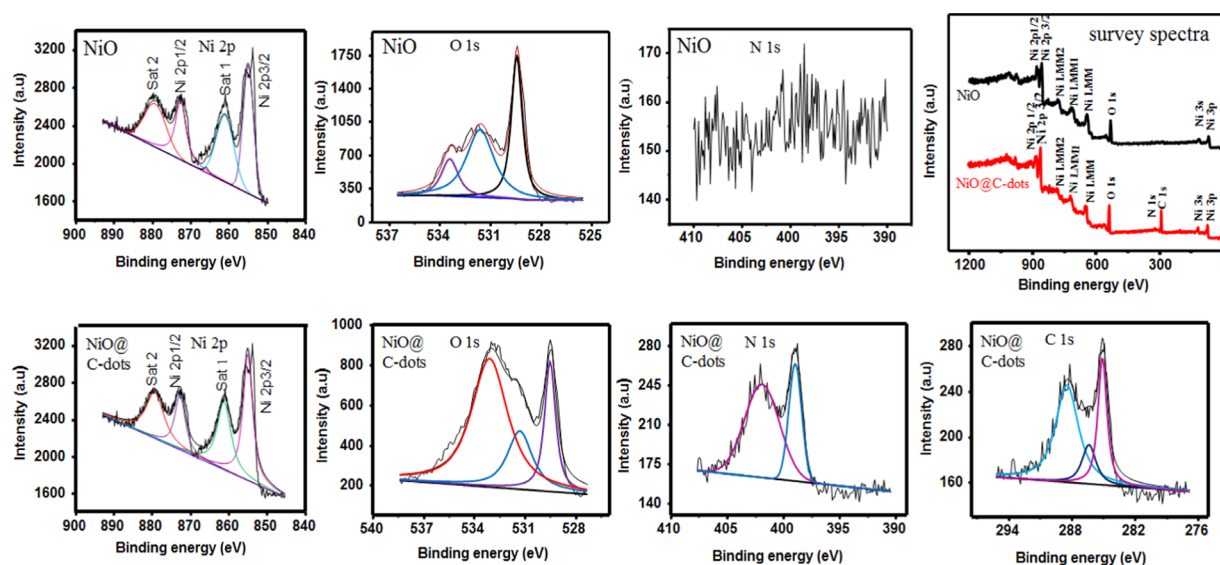


Figure 3. XPS survey spectra and XPS fine and deconvoluted spectra of C 1s, N 1s, O 1s, Ni 2p_{3/2}, and Ni 2p_{1/2} of NiO NPs and NiO@C-dots.

(222) with lattice constants of $a = 4.171 \text{ \AA}$ and $c = 2.912 \text{ \AA}$, which are consistent with a reported constant of $a = 4.175$ (JPCDS no. 01-1239).^{23,25} Incidentally, the XRD peaks of NiO@C-dots were very consistent with those of NiO NPs and new peaks did not appear because the addition of C-dots did not affect the crystallography of NiO NPs.²⁶

The XPS survey spectra of the NiO NPs and NiO@C-dots and their fine spectra are shown in Figure 3, confirming the presence of C 1s, N 1s, O 1s, and Ni 2p elements. The deconvoluted line spectra of fine peaks are also exhibited in Figure 3. The numerical values of binding energies and area intensities of deconvoluted families are compared in Table 1. Although NiO NPs did not have C 1s and N 1s peaks, NiO@C-dots had them; there were three deconvoluted peaks of C 1s at 285.0, 286.2, and 288.4 eV that were assigned to the C–C/C=C (aromatic ring), C–OOH/C–NH₂ (amine)/C–C–(alkyl), and C–OH bonds, respectively, having originated

from C-dots.^{27–29} Two deconvoluted N 1s peaks appeared at 400.0 and 402.0 eV and were attributed to C–NH₂ of C-dots.²⁶ O 1s and Ni 2p peaks were observed commonly for both NiO NPs and NiO@C-dots. Three deconvoluted peaks of O 1s appeared as bonds in NiO NPs and C-dots, that is, at 529.4 eV (Ni–O), 531.3 eV (Ni–OH/C=O), and 533.1 eV (OH(H₂O)/C–OH).²⁸ The characteristic Ni 2p (Ni 2p_{3/2} and Ni 2p_{1/2}) peaks appeared at strong twin peaks, corresponding to Ni–O and Ni–OH bonds, respectively, which prove the existence of NiO and Ni(OH)₂.³⁰ As seen in Table 1, the area intensities of C 1s binding energies of NiO@C-dots were highest for the 285.0 eV peak, indicating that the aromatic ring component was the majority in C-dots in comparison to other functional groups. The area intensities of O 1s bonds differently behaved between NiO NPs and NiO@C-dots: Those of NiO NPs were decreased from a 529.4 eV peak to a 533.4 eV peak, depending on the contribution of NiO, Ni–OH, and OH (H₂O). However, the relative area intensities of O 1s peaks of NiO@C-dots varied from those of NiO NPs because the contribution from C-dots was added to higher-binding-energy peaks. Thus, the analyses of XPS and FT-IR spectra confirm that C-dots are attached to NiO NPs.

Table 1. Binding Energies (BE), Their Area Intensities, and Their Assignments from XPS of NiO NPs and NiO@C-Dots

element	NiO		NiO@C-dots		assignment
	BE (eV)	area intensity (au)	BE (eV)	area intensity (au)	
C 1s			285.0	351	C–C/C=C (aromatic ring)
			286.2	170	C–OOH/C–N(amine)/C–C(alkyl)
			288.4	79	C–OH
N 1s			400.0	209	C–NH ₂
			402.0	423	C–NH ₂
O 1s	529.4	2337	529.4	741	Ni–O
	531.5	1369	531.3	640	C=O
	533.4	627	533.1	617	C–OH
Ni 2p _{3/2}	855.1	6253	855.2	4778	Ni ²⁺ (Ni–O)
	861.1	6681	861.2	5206	Ni ³⁺ (NiO) satellite
Ni 2p _{1/2}	872.4	3976	872.4	2428	Ni ²⁺ (Ni–OH)
	879.5	3840	879.5	3830	Ni ³⁺ (NiO) satellite

3.2. DSSC Performance. I – V curves for NiO DSSC were measured for different photosensitizers (Rh6G and N719). All measurements of power conversion efficiency (PCE) were made using a 430 nm LED source (50 mW/cm²). As shown in Figure 4, the current density decreased with increasing voltage and the PCE was evaluated to be 1.80 and 2.44%, respectively. These values were higher than the efficiencies obtained for a ZnO DSSC (0.10 and 0.80%, respectively) but still lower than those of other solar cells. However, it has been reported that the addition of C-dots to a ZnO DSSC enhances its PCE.²⁰ Thus, C-dots were added in the present investigation. Figure 4 shows the I – V curves of NiO@C-dots at various C-dot contents (at EDA/CA = 1:1 molar ratio), and the parameters for the DSSC depending on the C-dot contents in the NiO@C-dots were evaluated, as listed in Table 2 and plotted in Figure 4. All of the parameters (short-circuit current density, open-circuit voltage, fill factor, and PCE) depended on the C-dot content. These parameters increased with increasing C-dot content up to 12.5 wt % but decreased following the addition

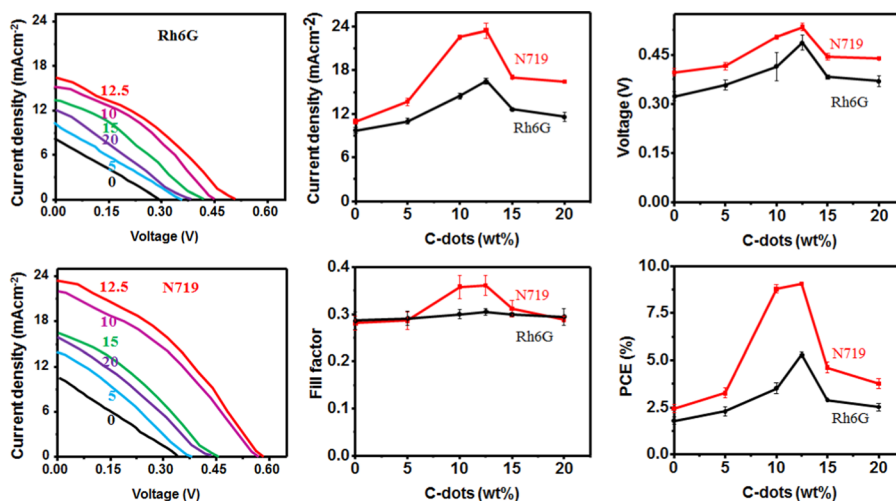


Figure 4. *I*–*V* curves and calculated electrochemical parameters of NiO@C-dots DSSCs at 1:1 EDA/CA molar ratio at different C-dot contents and sensitizers. The numerals in the *I*–*V* curves indicate C-dot contents in wt % unit.

Table 2. Electrochemical Parameters Calculated from *I*–*V* Curves of NiO@C-dots DSSCs in Figure 4 (A) at Different C-dot Contents at 1:1 EDA/CA Molar Ratio and (B) at Different EDA/CA Molar Ratios at 12.5 wt % C-dot Content^a

	current density (mA/cm ²)		voltage (V)		fill factor		PCE (%)	
	Rh6G	N719	Rh6G	N719	Rh6G	N719	Rh6G	N719
(A) C-Dot Content (wt %)								
0	10.2 ± 0.4	11.2 ± 0.4	0.32 ± 0.01	0.39 ± 0.01	0.28 ± 0.01	0.28 ± 0.02	1.82 ± 0.09	2.44 ± 0.21
5	11.0 ± 0.4	13.4 ± 0.5	0.36 ± 0.02	0.42 ± 0.01	0.29 ± 0.02	0.29 ± 0.02	2.29 ± 0.23	3.27 ± 0.27
10	14.0 ± 0.4	21.9 ± 0.3	0.42 ± 0.04	0.51 ± 0.01	0.30 ± 0.01	0.36 ± 0.03	3.52 ± 0.29	8.04 ± 0.51
12.5	16.9 ± 0.4	22.6 ± 1.2	0.49 ± 0.02	0.53 ± 0.01	0.31 ± 0.01	0.36 ± 0.02	5.13 ± 0.33	8.62 ± 0.37
15	12.5 ± 0.1	14.4 ± 0.2	0.38 ± 0.01	0.44 ± 0.01	0.30 ± 0.00	0.31 ± 0.03	2.85 ± 0.13	3.93 ± 0.33
20	11.6 ± 0.6	14.8 ± 0.1	0.37 ± 0.02	0.44 ± 0.00	0.29 ± 0.02	0.29 ± 0.01	2.50 ± 0.19	3.77 ± 0.26
(B) Ratio of EDA/CA								
0.5:1	10.3 ± 0.4	12.7 ± 0.5	0.35 ± 0.03	0.38 ± 0.04	0.28 ± 0.01	0.31 ± 0.01	2.01 ± 0.14	3.00 ± 0.36
1.0:1	16.9 ± 0.4	23.4 ± 0.1	0.48 ± 0.02	0.54 ± 0.02	0.31 ± 0.01	0.36 ± 0.02	5.03 ± 0.33	9.10 ± 0.36
1.5:1	16.6 ± 1.1	23.6 ± 0.8	0.48 ± 0.01	0.58 ± 0.02	0.34 ± 0.02	0.36 ± 0.01	5.41 ± 0.42	9.85 ± 0.46
2.0:1	16.8 ± 0.6	22.7 ± 0.5	0.48 ± 0.01	0.54 ± 0.01	0.31 ± 0.01	0.37 ± 0.03	5.19 ± 0.34	9.10 ± 0.39
2.5:1	11.4 ± 0.6	15.2 ± 0.1	0.36 ± 0.01	0.45 ± 0.02	0.29 ± 0.01	0.26 ± 0.02	2.38 ± 0.10	3.55 ± 0.32

^aExperiments were performed under 430 nm blue LED excitation with 50 mW/cm².

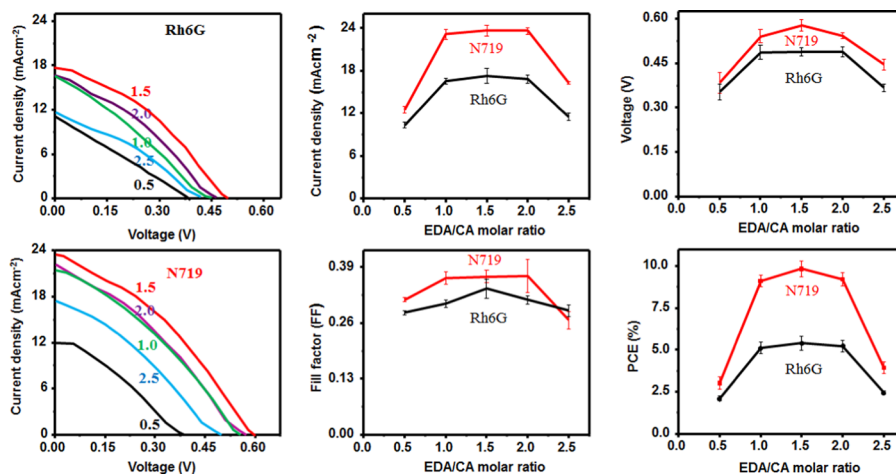


Figure 5. *I*–*V* curves and calculated electrochemical parameters of NiO@C-dots DSSCs at different EDA/CA molar ratios at 12.5 wt % C-dot content. The numerals in *I*–*V* curves indicate EDA/CA mole ratio.

of further C-dots. Therefore, all of these parameters were the highest at a C-dot content of 12.5 wt %, and the parameters of the N719 DSSC were always higher than those of the Rh6G

DSSC. As revealed in Table 2, the PCE of NiO@C-dots for the N719 DSSC at a C-dot content of 12.5 wt % was 4 times that of NiO and 2 times that of Rh6G DSSC, which indicates the

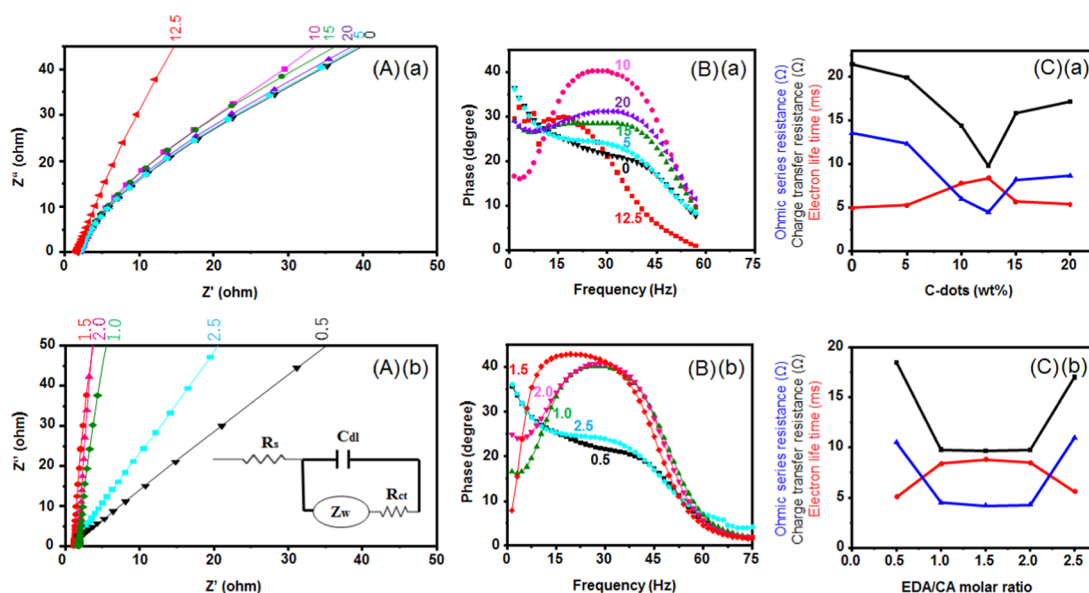


Figure 6. (A) Nyquist plots and (B) Bode phase plots of EIS of NiO@C-dots (a) at different C-dots contents at 1:1 EDA/CA molar ratio and (b) at different EDA/CA molar ratios at 12.5 wt % C-dot content. The numerals indicate (a) C-dot content in wt % and (b) EDA/CA molar ratio. (C) Plots of ohmic series resistance, charge transfer resistance, and electron lifetime as a function of EDA/CA molar ratio.

Table 3. Parameters Obtained from EIS, Tauc Plots, N₂ Adsorption–Desorption Isotherms, and N719 Adsorption of NiO@C-dots (A) at Different C-Dot Contents (at 1:1 EDA/CA Molar Ratio) and (B) at Different EDA/CA Molar Ratios (at 12.5 wt % C-Dot Content)

R_s (Ω)	R_{ct} (Ω)	τ_e (ms)	band gap (eV)	type	specific surface area (m^2/g)	pore diameter (nm)	pore volume (cm^3/g)	N719 adsorption (mg/mg)
(A) C-Dot Content (wt %)								
0	13.56	21.45	4.98	III	38.7	23.38	0.227	0.295
5	12.33	19.95	5.30	IV	43.5	21.42	0.231	0.296
10	6.02	14.45	7.80	IV	58.8	9.75	0.152	0.466
12.5	4.51	9.80	8.40	IV	61.3	9.46	0.145	0.525
15	8.23	15.84	5.70	IV	57.2	9.97	0.143	0.325
20	8.67	17.20	5.41	IV	53.8	10.34	0.215	0.298
(B) EDA/CA Molar Ratio								
0.5:1	10.51	18.45	5.10	III	41.2	31.97	0.275	0.309
1.0:1	4.51	9.80	8.40	IV	61.3	9.46	0.145	0.525
1.5:1	4.20	9.70	8.80	IV	78.9	7.69	0.127	0.589
2.0:1	4.28	9.78	8.50	IV	65.4	8.41	0.137	0.541
2.5:1	11.01	17.01	5.60	II	54.9	20.33	0.279	0.345

high effectiveness of C-dots in the composite, especially for the NiO@C-dots/N719 DSSC.

Figure 5 displays the I – V curves for NiO@C-dots DSSCs at a 12.5 wt % C-dot content but various EDA/CA molar ratios of 0.5:1, 1.0:1, 1.5:1, 2.0:1, and 2.5:1 for the N719 and Rh6G sensitizers. Electrochemical parameters evaluated from these I – V curves are listed in Table 2 and plotted in Figure 5. Four parameters were influenced by the EDA/CA molar ratio for both sensitizers: All parameters were commonly highest at an EDA/CA molar ratio of 1.5:1 and higher for N719 DSSC than for Rh6G DSSC, suggesting the effect of the amine (NH_2) moiety in the C-dots since the increase in the EDA/CA molar ratio enhances the amine content relative to the carboxylic acid content. As seen in Table 2, the highest power conversion efficiency (9.85%) was achieved at a 1.5:1 EDA/CA molar ratio in C-dots for the NiO@C-dots/N719 DSSC with a 12.5 wt % C-dot content.

3.3. Effect of Carbon Dots. The effect of C-dots on a NiO-based DSSC should be related to the charge transfer

resistance, band gap, surface property, and sensitizer adsorption. The EIS of NiO@C-dots was measured over a frequency range of 1–100 Hz at an amplitude of 10 mV, and the Nyquist plot for evaluating the ohmic series resistance (R_s) and charge transfer resistance (R_{ct}) is shown in Figure 6A. The EIS results were also plotted as a Bode phase plot, as shown in Figure 6B, and the electron lifetime (relaxation time) (τ_e) was evaluated from this plot as a peak in the Bode phase plot.³¹ The numerical values of the parameters from the two plots are collected in Table 3 and plotted in Figure 6 for DSSCs with varying C-dot contents (at a 1:1 EDA/CA molar ratio) and different EDA/CA molar ratios (at 12.5 wt % C-dots content). A C-dot content of 12.5 wt % and an EDA/CA molar ratio of 1.5 led to the lowest resistance value and the highest electron lifetime. These tendencies were consistent with the maximum PCE observed at a C-dot content of 12.5 wt % and an EDA/CA molar ratio of 1.5. These results imply that the higher PCE occurred under the condition of faster charge transfer, which is expected to reduce charge (electron–hole) recombination.

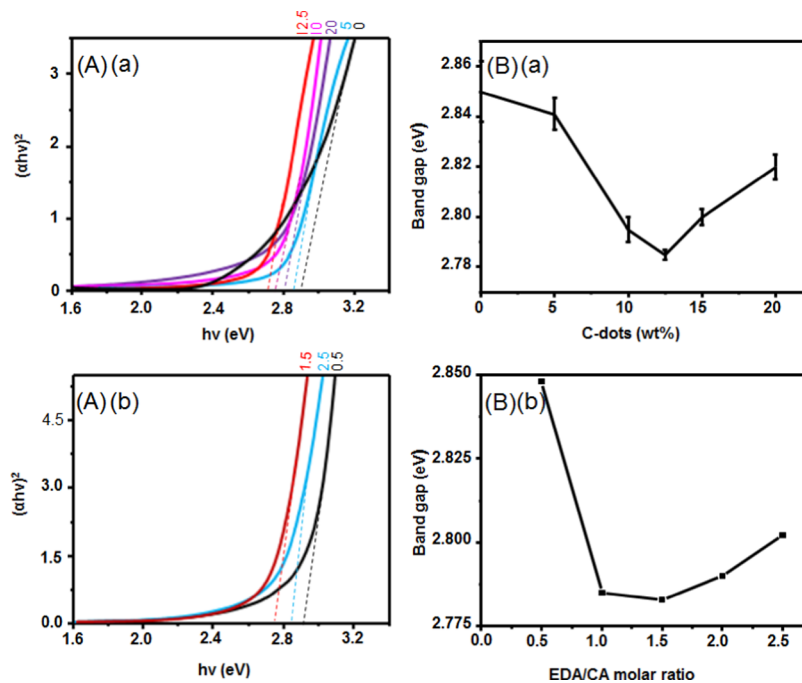


Figure 7. (A) Tauc plots of UV–vis absorption spectra of NiO@C-dots and (B) plots of band gap (a) at different C-dot contents (at 1:1 EDA/CA molar ratio) and (b) at different EDA/CA mole ratios (at 12.5 wt % C-dot content). The numerals in Tauc plots indicate (a) C-dot content in wt % and (b) EDA/CA molar ratio.

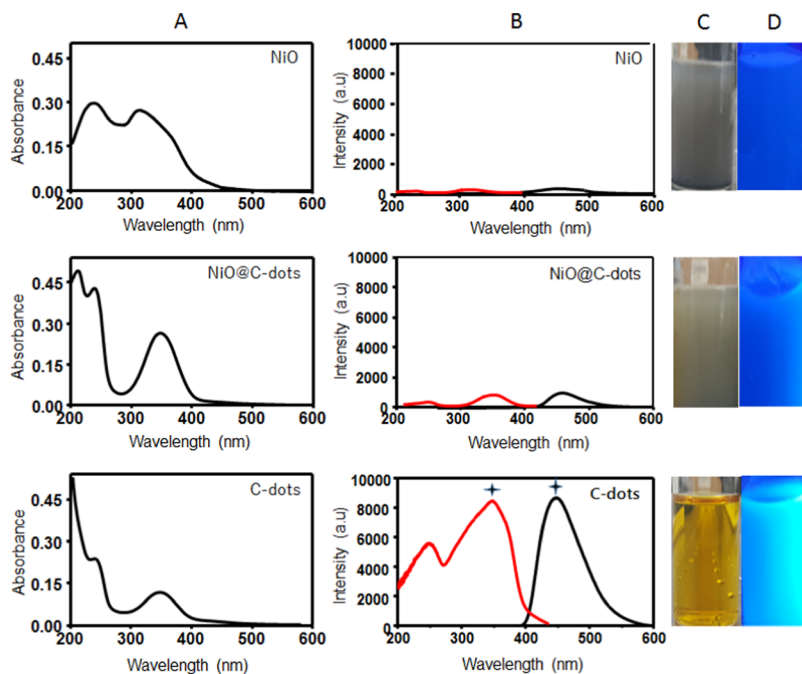


Figure 8. (A) UV–vis absorption spectra, (B) photoluminescence (PL) spectra, and (C, D) photographs of aqueous dispersions of NiO, NiO@C-dots, and C-dots at a concentration of 0.2 mM. (Red) Excitation spectrum and (black) emission spectrum in the PL spectra (C) without and (D) with black light.

The optical energy gap (E_g) of the composites composed of NiO NPs with C-dots can be evaluated from the Tauc plot of the UV–vis absorption spectrum using the equation $(\alpha h\nu)^2 = \beta(h\nu - E_g)$, where α is the optical absorption coefficient that is calculable from the thickness of a conductive specimen; its absorbance, $h\nu$, is the photon energy calculated from the wavelength, and β is a constant related to the material.³² From the plot of $(\alpha h\nu)^2$ as a function of $h\nu$ (Figure 7), when the

straight line in the plot was extrapolated to $(\alpha h\nu)^2 = 0$, the energy band gaps of the NiO NPs with different C-dot contents and EDA/CA molar ratios were obtained, as listed in Table 3 and plotted in Figure 7. Obviously, the energy band gap of the NiO@C-dots was reduced when C-dots at a 1:1 EDA/CA molar ratio were added up to the contents of 12.5 wt %; however, this energy band gap increased with the addition of further C-dots above this content. Similarly, as seen in

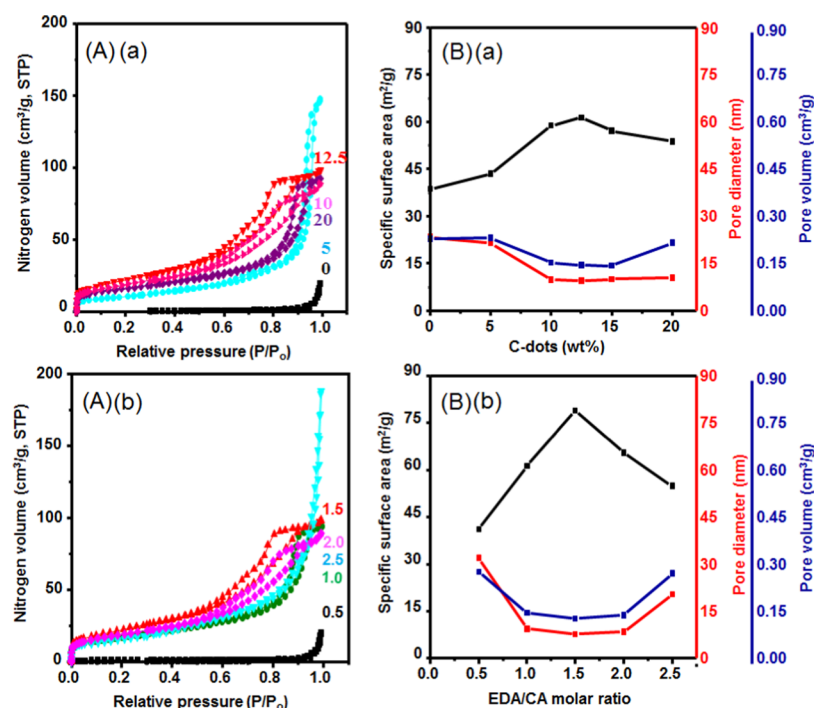


Figure 9. (A) N_2 adsorption–desorption isotherms of NiO@C-dots and (B) plots of parameters from isotherms (a) at different C-dot contents (at 1:1 EDA/CA molar ratio) and (b) at different EDA/CA molar ratios (at 12.5 wt % C-dot content). The numerals in isotherms indicate (a) C-dot content and (b) EDA/CA molar ratio.

Figure 7 and Table 3, the energy band gap of the NiO@C-dots at a 12.5 wt % C-dot content was minimized at a 1.5 EDA/CA molar ratio in the C-dots. These tendencies for the band gap coincide with the variation in the PCE described above. Hence, it can be expected that the variation in the band gap of the NiO NPs due to the attachment of C-dots modifies the electronic and optical properties and DSSC performance of NiO.³³ As seen in Table 3, the energy band gap of NiO was shortened from 2.85 eV for C-dot-free NiO NPs to a minimum value of 2.78 eV after the addition of C-dots, although band gaps of 2.2–2.7 eV have been reported for nitrogen-doped carbon quantum dots synthesized using microplasma.³⁴ Thus, the binding of C-dots to metal oxides in photovoltaic cells is effective in decreasing the band gap of the semiconductors.

Figure 8A shows UV–vis absorption spectra of NiO NPs, NiO@C-dots, and C-dots in aqueous dispersions. The absorption bands of the C-dots appear at 250 and 360 nm, which can be assigned to the electron transition modes of $\pi-\pi^*$ and $n-\pi^*$, respectively.³⁵ On the other hand, the absorption band of NiO at 320 nm is attributed to the electronic transition from the valence band to the conductive band.^{36,37} Then, the absorption bands of the NiO@C-dots appeared at 353 and 250 nm, although the 353 nm band was slightly shifted from the $n-\pi^*$ band of the C-dots.

It is known that C-dots are a strongly fluorescent substance.³⁸ Thus, the photoluminescence (PL) of C-dots may support the interaction of C-dots with NiO NPs. The PL spectra obtained for NiO NPs, NiO@C-dots, and C-dots are shown in Figure 8B. When aqueous dispersions of C-dots were excited at 250 and 360 nm, their corresponding emission band was observed at 447 nm. As the intensity of the excitation band at 360 nm was strong and comparable to that of an emission band, the emission band at 447 nm mainly originates from the excitation at 360 nm. The PL bands of NiO@C-dots were 1

order weaker than those for C-dots, although the excitation and emission bands were located at similar wavelengths. Incidentally, the PL bands of the NiO NPs were vanishingly small; that is, NiO NPs should have no intrinsic PL. These differences were apparent from the observation of the dispersions under black light. The pictures of solutions with and without black light are displayed in Figure 8C. Against the strong fluorescent blue color of the aqueous dispersion of C-dots, the NiO@C-dot dispersions showed a very weak blue color, and the NiO NPs displayed no blue color.

It should be assumed that the light energy adsorbed by C-dots is intrinsically released through the process of fluorescence emission; however, this can lead to charge separation by the effect of light harvesting without emission, and the photoinduced electrons are transferred to the NiO NPs when C-dots are bound to the NiO NPs. Then, C-dots can donate energy to the NiO acceptor.^{39,40} As a result of their strong light-harvesting property, C-dots lead to promising photogenerated charge separation, high electron mobility, and thus a reduction in the electron–hole recombination, which finally contribute to a high PCE by increasing the dye adsorption and photocurrent generation. The light-harvesting and electron donor/acceptor properties of C-dots have been demonstrated and used in photocatalysts, photosensitizers, and photovoltaic devices.^{20,41}

The N_2 adsorption–desorption isotherms of NiO@C-dots at different C-dot contents (at a 1:1 EDA/CA molar ratio) and at different EDA/CA molar ratios (at a 12.5 wt % C-dots contents) are shown in Figure 9A; the specific surface area was analyzed using the Brunauer–Emmett–Teller (BET) method, and the pore diameter and volume were determined using the Barrett–Joyner–Halenda (BJH) method. The numerical values are listed in Table 3 and plotted in Figure 9B. All of the isotherms were found to be of type IV except for the

NiO@C-dots with zero C-dot content (at an EDA/CA molar ratio of 1:1) and those at an EDA/CA molar ratio of 0.5 (at a 12.5 wt % C-dot content), for which the isotherms were of type III, and the NiO@C-dots at an EDA/CA molar ratio of 2.5 (with a 12.5 wt % C-dot content), for which the isotherms were of type II. The specific surface area displayed a maximum at the C-dot contents of 12.5 wt % and the EDA/CA molar ratio of 1.5. However, the pore diameter and volume were minimized under these conditions, which is the same as the condition of the maximized PCE. Most likely, the coexistence of C-dots and NiO NPs brings about an increase in the surface area of the composite due to the increased surface roughness induced by the binding of C-dots. However, the strong adsorption of C-dots onto the NiO NP surface may reduce the pore size and volume. Eventually, the increased surface area was effective in increasing the PCE of the NiO@C-dots DSSC, as it allows easy adsorption of the sensitizer and facilitates the approach of electrolytes.

The adsorbed amount of sensitizer is an important factor that governs the PCE of a DSSC. The amount of sensitizer adsorbed (N719) on the NiO@C-dots was measured, as listed in Table 3 and plotted in Figure 10. The amount of adsorbed

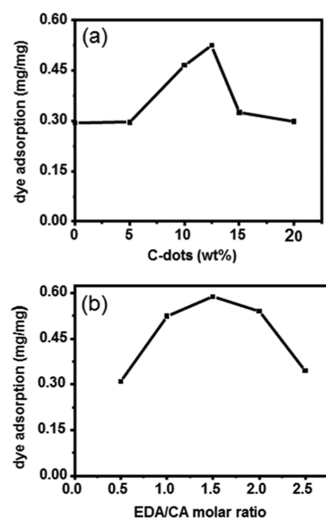


Figure 10. Adsorption amounts of N719 on NiO@C-dots (a) at different C-dots contents (at 1:1 EDA/CA molar ratio) and (b) at different EDA/CA molar ratios (at 12.5 wt % C-dot content).

sensitizer was the highest at the C-dots content of 12.5 wt % and the EDA/CA molar ratio of 1.5:1. Thus, this result shows that a higher adsorption amount of sensitizer is more favorable for light harvesting, which is the main and most important factor in DSSC performance. In fact, the highest adsorption amount of sensitizer occurred under the same condition for the C-dot species as did the highest PCE for the NiO@C-dots. The increase in the C-dot content promotes an increase in the PCE of the DSSC since the amount of light-harvesting materials increases. However, the adsorption of more than 12.5 wt % C-dots extensively covers the surface of NiO and blocks, that is, decreases, the adsorption of dye on NiO. A similar phenomenon and explanation have been reported in the case of a ZnO@C-dot DSSC.²⁰

It was experimentally proved that the adsorption ability of N719 on C-dots@ZnO was higher than that of rhodamine B.²⁰ Similarly, while the adsorption of N719 on the C-dots@NiO electrode at a 12.5 wt % C-dot content (1.5:1 EDA/CA molar

ratio) was 0.589 mg/mg (electrode), as listed in Table 3, the adsorption of Rh6G on the same electrode was 0.315 mg/mg (electrode). The N719 dye has four carboxylic acid groups, while Rh6G has only one carboxylic acid group. These carboxylic acid groups play a crucial role in anchoring or stabilizing the dyes on semiconductors, such as ZnO and NiO, perhaps through hydrogen bonding. Thus, N719 has better adsorption ability than Rh6G.

In the present NiO@C-dot DSSC systems, the best photovoltaic performance was achieved by the ITO electrode coated by semiconductive NiO NP materials and sensitized by N719 with a C-dot content of 12.5 wt % and an EDA/CA molar ratio of 1.5 bound onto NiO NPs. Moreover, N719 was more effective as a sensitizer than Rh6G, as explained above, and the photovoltaic performance of the NiO@C-dots DSSC systems was found to be proportional to the amount of N719 adsorbed, indicating that the amount of sensitizer is the most important factor. This amount should be regulated by the attachment of C-dots onto the NiO NPs, which arises from the simple mixing of C-dots with NiO NPs. The binding of C-dots increased the surface area of the composite due to the increased surface roughness. This increase is effective in creating a binding functional group for the sensitizer and in raising the PCE of the NiO@C-dots DSSC for two reasons: the easy adsorption of the sensitizer and the facile approach of electrolytes. In particular, the amine group should be the effective binding group because the increase in the EDA/CA molar ratio, that is, the increase in the ratio of amine groups to carboxylic acid groups, is confirmed. It was reported that amine (N) doping in C-dots can shift the energy gap as well as promote charge separation.^{32,35} However, the excess addition of C-dots degrades the photovoltaic performance and sensitizer adsorption due to the decreased specific surface area of the NiO@C-dots caused by the attachment of excess C-dots onto the NiO NPs.²¹

At the maximum NiO@C-dots DSSC performance, as evidenced by the EIS results, the charge transfer becomes fast, and therefore, the charge (electron–hole) recombination is expected to be reduced. At the same time, the effective decrease in the band gap due to the binding of C-dots to NiO NPs in the photovoltaic cell also facilitates charge (electron–hole) separation. Both the reduction in charge recombination and the facilitation of charge separation result in enhanced solar cell performance. The PL behavior revealed a drastic reduction in the PL bands of the C-dots after their binding onto the NiO NPs. This result suggested that the light energy harvested by the C-dots was transferred to the NiO NPs and that this phenomenon contributed to the reduction in the band gap. The smaller band gap observed after the addition of C-dots is responsible for the easier and more abundant charge separation, and this phenomenon leads to minimization of the carrier recombination.

The energy levels of the valence and conduction bands of NiO NPs are reported to be -5.1 and -2.1 eV, respectively,⁴² and the reported highest occupied molecular orbital (HOMO) and lowest occupied molecular orbital (LUMO) levels of C-dots are -7.13 and -3.52 eV, respectively.⁴³ Then, the HOMO and LUMO levels of C-dots are positioned below the valence and conduction bands of NiO NPs, respectively. When the photoenergy is provided, the photoharvesting C-dots give rise to the charge separation (electron–hole separation) and the valence band of p-type NiO NPs receives holes from the HOMO level of C-dots. This fact could shift the Fermi level

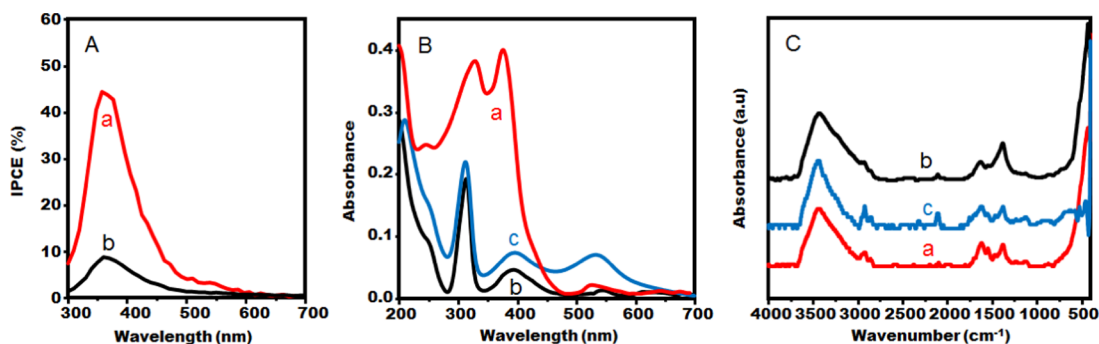


Figure 11. (A) IPCE plots, (B) UV-vis absorption spectra of ethanol solutions, and (C) infrared absorption spectra of (a) NiO@C-dots/N719 (at 12.5 wt % C-dot content and 1.5:1 EDA/CA molar ratio), (b) NiO/N719, and (c) N719.

toward the valence band of the p-type composites (NiO@C-dots)⁴⁴ and then shrink the valence and conduction bands of NiO NPs after attached by C-dots, giving rise to the lowering of energy gap and Fermi level of composites as a result.

The spectral sensitivity, as well as the PCE, is an important tool for assessing the solar cell performance. The incident photon-to-current conversion efficiency (IPCE) plots (Figure 11A) indicated that the IPCE of NiO@C-dots/N719 at 12.5 wt % C-dot and 1.5:1 EDA/CA molar ratio was higher than that of NiO/N719 since their maximum IPCE values were 45.1 and 9.3%, respectively, at 362 nm wavelength. The IPCE value under the light source of wavelength λ and incident intensity P_{in} can be calculated using the short-circuit current density J_{sc} value evaluated from the I - V curve based on the following equation⁴⁵

$$IPCE(\lambda) = \frac{\left(\frac{J_{sc}}{e}\right)}{\text{photon flux}} \quad (3)$$

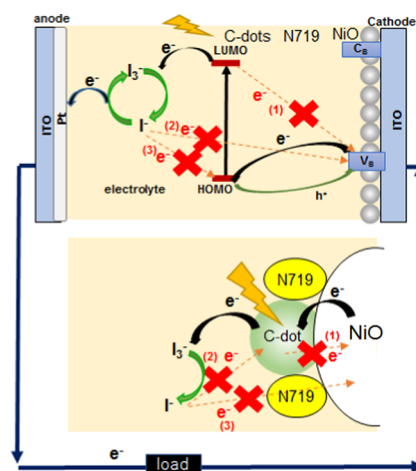
where e is the charge of the electron, photon flux = $P_{in}\lambda/hc$, h is Planck's constant, and c is the light speed. The relevant IPCE value of NiO@C-dots/N719 (at 12.5 wt % C-dot content and 1.5:1 EDA/CA molar ratio), calculated with a 430 nm light source of 50 mW/cm² light intensity using eq 3 and the J_{sc} value in Table 2, was 13.6%, higher than the 6.4% value of NiO/N719. These values were relatively consistent with the observed IPCE values at 430 nm in Figure 11A, which were 16.2 and 5.1%.

It should be noted that the IPCE spectra of both NiO@C-dots/N719 and NiO/N719 presented a maximum at 362 nm (Figure 11A). These spectra are different from the typical IPCE spectra, centered on 500 nm for the N719 sensitized solar cells,⁴⁵ although the present IPCE spectra have a tail above 500 nm (Figure 11A). When these IPCE spectra are compared to the UV-vis absorption spectra of NiO@C-dots/N719, NiO/N719, and N719 as shown in Figure 11B, NiO/N719 displays similar absorption bands at 313, 390, and 530 nm matching that of N719 alone, but a spectrum of NiO@C-dots/N719 also presents a strong new band at 375 nm. This new band corresponds to that of C-dots, as estimated by comparison of the UV-vis absorption spectra of NiO, NiO@C-dots, and C-dots without N719 (Figure 8A). Thus, it can be interpreted from the similarity of the UV-vis absorption and IPCE spectra in the shape and position that the IPCE spectrum of NiO@C-dots/N719 received a greater contribution from absorption bands of C-dots and NiO than from the metal-ligand charge transfer band of N719. This strong contribution of C-dots to IPCE is consistent with the

contribution estimates for C-dots to PCE, as described above. Similar N719-noncontributed IPCE spectra have been reported for the PbS quantum dot-N719 solar cells.⁴⁶

The p-type DSSC is illustrated in Scheme 1, where the working electrode (cathode) is constructed from ITO, NiO

Scheme 1. Schematic Illustration of a NiO/C-Dots/N719 Solar Cell



NP, C-dot, and dye components. When the visible light is irradiated to a sensitizer, the electrons are excited from the ground state (HOMO) to a lower unoccupied molecular orbit (LUMO). The sensitizer then injects a photogenerated electron into the electrolytes, and the electron is transferred to a counter electrode (anode) via the redox process between the electrolytes (I_3^-/I^-) before moving to the working electrode (cathode) through an external circuit. In the present case, C-dots were selectively sensitized by the visible light, clarified from the IPCE spectrum. To determine if C-dots would mainly reveal the sensitization on NiO solar cells to a greater extent than N719, the FT-IR spectra of N719, NiO/N719, and NiO@C-dots/N719 were measured (Figure 11C). The spectra indicated that N719 presented characteristic IR bands at 3465, 2930, 2856, 2150, 1630, 1536, and 1376 cm⁻¹ assigned to OH stretching, CH antisymmetric stretching, CH symmetric stretching, isothiocyanate ($-N=C=S$, NCS), COO⁻ antisymmetric stretching, bipyridine C=C, and COO⁻ symmetric stretching bands, respectively.^{47,48} Although these bands could also be observed in NiO/N719 and NiO@C-dots/N719, their relative intensities varied; then, the absorbance ratio of the NCS band versus the COO⁻

Table 4. Comparison of Semiconductor Solar Cells Co-adsorbed by Quantum Dots and N719

sensitizer	quantum dot (QD)	N719	QD/N719		
metal oxide		PCE (%)		main peak in IPCE ^a	refs
TiO ₂		5.95	6.35 (PbSQD)	350 nm	46
TiO ₂	0.177 (N ₃₀₀ -CQD)	8.09	9.29 (N ₃₀₀ -CQD)		56
TiO ₂		6.28	6.90 (G-CD)		57
TiO ₂	0.208 (N-CQD/CQD/S-CQD)	6.90	9.04 (N-CQD/CQD/S-CQD)	365 nm, 425 nm, 480 nm, 550 nm	58
ZnO	0.001 (CQD)	0.80	5.92 (CQD)		20
NiO	0.152 (CQD)	2.44	9.85 (CQD)	362 nm	present

^aWavelengths of main peaks in the IPCE plot are listed.

symmetric stretching band decreased from 0.76 (N719) to 0.36 (NiO/N719), and decreased further to 0.29 (NiO@C-dots/719). These variations indicate the strong interactions of the NCS species in N719 with NiO and C-dots. The strong interaction of NCS in N719 with NiO disrupts N719 interactions with electrolytes (I^-/I_3^-) and electron interchanges between them.⁴⁹ Moreover, strong NCS interactions accelerate positive electron transfers from C-dot LUMO to I^-/I_3^- and from the NiO valence band to the C-dot HOMO. By contrast, it inhibits negative electron transfers, which encompass (1) the process that combines an excited electron on C-dot LUMO with a NiO hole, (2) the process that combines an electron released from I^- with a NiO hole, and (3) the process that combines an electron released from I^- with a C-dot HOMO hole, as described in Scheme 1.

The PCE of DSSCs is generally low compared to that of other solar cells,⁵⁰ and the PCE of a p-type DSSCs is especially lower than that of an n-type DSSC.⁵¹ The PCE of carbon quantum dot solar cells is also extremely low different from metal compound-based quantum dot solar cells.^{52–55} However, the present research has confirmed that the p-type DSSC performance was enhanced remarkably, when two photosensitizers (dye and C-dots) coexisted. The results of recent research of DSSC co-sensitized by N719 and quantum dots are listed in Table 4.^{20,46,56–59} Liu and Wang⁴⁶ investigated TiO₂/PbS quantum dot/N719 DSSCs, and three other groups^{56–58} reported results on TiO₂/carbon quantum dot/N719 DSSCs. In their cases, the enhancement effect of quantum dots on TiO₂/N719 DSSCs was only 1.1–1.3 times, although the effect of N719 on a TiO₂/quantum dot solar cells was larger or the effect of quantum dots and N719 on TiO₂ solar cells was rather additive. The present NiO/N719 DSSC differed by being enhanced strongly (roughly 4.0 times) after adding C-dots. A similar phenomenon (7.4 times enhancement) happened with the addition of C-dots to ZnO/N719 DSSC. Moreover, the effects of quantum dots and N719 on NiO solar cells were not additive but a synergistic action. The difference between NiO-based solar cells and TiO₂-based solar cells should come from the differing sensitizing mechanisms of C-dots and N719, as estimated from the IPCE spectra. The logic behind such difference will be discussed in the following.

4. CONCLUSIONS

In summary, composites composed of C-dots and NiO NPs were synthesized by just mixing an appropriate ratio of C-dots with NiO NPs. C-dots scarcely exhibit a photovoltaic effect,^{20,60} and NiO-based DSSCs show a low PCE value due to the rapid charge recombination in the NiO semiconductor. However, once an adequate content of C-dots was combined with NiO NPs, the PCE performance of NiO NPs in DSSCs

was drastically improved. Primarily, this phenomenon can happen due to the abundant charge separation, reduction in charge recombination because of the reduced band gap of the composite, and the increased N719 adsorption of the composites after the addition of C-dots. It should be noted that the C-dots played mainly the sensitizing role in the DSSC and N719 behaved as an accelerator of the positive electron transfer and a restrainer of the electron–hole recombination. This should be the distinctive sensitizing mechanism of the carbon quantum dot-N719-sensitized p-type solar cells.

In our present investigation, a DSSC fabricated based on a composite of NiO NPs with C-dots using N719 achieved a PCE of 9.85% at an EDA/CA molar ratio of 1.5:1 and the C-dots content of 12.5 wt %. It has been recently reported that a similar enhancement occurs even for a ZnO DSSC, where the PCE (5.9%) of the ZnO@C-dot DSSC was far better than that of a ZnO DSSC.²⁰ Therefore, it can be noted that C-dots commonly influence both p-type and n-type DSSCs and that they show the promising enhancement in the DSSC device performance, which is strongly related to the improvement in the PCE of these solar cells. Among different types of solar cells, the DSSC shows a low PCE and short lifetime. However, it has the merits of low cost, compactness, and facile production. It is also repaired easily and cheaply following breakage. Hence, the unique demands for carbon quantum dot-DSSCs suggest that further improvements are expected.

■ ASSOCIATED CONTENT

Supporting Information

The Supporting Information is available free of charge at <https://pubs.acs.org/doi/10.1021/acsami.0c02413>.

TEM image of C-dots at 1.5:1 EDA/CA molar ratio (PDF)

■ AUTHOR INFORMATION

Corresponding Author

Toyoko Imae – Graduate Institute of Applied Science and Technology, Department of Chemical Engineering, and Department of Materials Science and Engineering, National Taiwan University of Science and Technology, Taipei 10607, Taiwan, Republic of China; orcid.org/0000-0003-2731-1960; Phone: +886-2-2730-3627; Email: imae@mail.ntust.edu.tw

Authors

Habtmu Fekadu Etefa – Graduate Institute of Applied Science and Technology, National Taiwan University of Science and Technology, Taipei 10607, Taiwan, Republic of China
Masatoshi Yanagida – National Institute for Materials Science (NIMS), Tsukuba 305-0044, Japan

Complete contact information is available at:
<https://pubs.acs.org/10.1021/acsami.0c02413>

Notes

The authors declare no competing financial interest.

ACKNOWLEDGMENTS

This investigation was partly supported by the Ministry of Science and Technology, Taiwan (MOST 107-2221-E-011-067-). H.F.E. fully acknowledges and appreciates the National Taiwan University of Science and Technology, Taiwan, for financial support and Ph.D. student scholarship. The authors thank Prof. M. Ujihara, Dr. M. T. Efa, and K. Wicaksono at the National Taiwan University of Science and Technology, Taiwan, for their technical assistance. The authors also thank Dr. Y. Shirai, National Institute for Materials Science (NIMS), Japan, for his valuable suggestion.

REFERENCES

- (1) Ranganathan, P.; Sasikumar, R.; Chen, S.-M.; Rwei, S.-P.; Sireesha, P. Enhanced Photovoltaic Performance of Dye-Sensitized Solar Cells Based on Nickel Oxide Supported on Nitrogen-Doped Graphene Nanocomposite as a Photoanode. *J. Colloid Interface Sci.* **2017**, *504*, 570–578.
- (2) Wu, J.; Lan, Z.; Lin, J.; Huang, M.; Huang, Y.; Fan, L.; Luo, G.; Lin, Y.; Xie, Y.; Wei, Y. Counter Electrodes in Dye-Sensitized Solar Cells. *Chem. Soc. Rev.* **2017**, *46*, 5975–6023.
- (3) Kashif, M. K.; Axelson, J. C.; Duffy, N. W.; Forsyth, C. M.; Chang, C. J.; Long, J. R.; Spiccia, L.; Bach, U. A New Direction in Dye-Sensitized Solar Cells Redox Mediator Development: In Situ Fine-Tuning of the Cobalt(II)/(III) Redox Potential through Lewis Base Interactions. *J. Am. Chem. Soc.* **2012**, *134*, 16646–16653.
- (4) Yang, J.; Bark, C.; Kim, K.; Choi, H. Characteristics of the Dye-Sensitized Solar Cells Using TiO₂ Nanotubes Treated with TiCl₄. *Materials* **2014**, *7*, 3522–3532.
- (5) Ahmad, W.; Chu, L.; Al-Bahrani, M. R.; Ren, X.; Su, J.; Gao, Y. P-type NiO Nanoparticles Enhanced Acetylene Black as Efficient Counter Electrode for Dye-Sensitized Solar Cells. *Mater. Res. Bull.* **2015**, *67*, 185–190.
- (6) Islam, A.; Akhtaruzzaman, M.; Chowdhury, T. H.; Qin, C.; Han, L.; Bedja, I. M.; Stalder, R.; Schanze, K. S.; Reynolds, J. R. Enhanced Photovoltaic Performances of Dye-Sensitized Solar Cells by Co-Sensitization of Benzothiadiazole and Squaraine-Based Dyes. *ACS Appl. Mater. Interfaces* **2016**, *8*, 4616–4623.
- (7) Hashem, M.; Saion, E.; Al-Hada, N. M.; Kamari, H. M.; Shaari, A. H.; Talib, Z. A.; Paiman, S. B.; Kamarudeen, M. A. Fabrication and Characterization of Semiconductor Nickel Oxide (NiO) Nanoparticles Manufactured Using a Facile Thermal Treatment. *Res. Phys.* **2016**, *6*, 1024–1030.
- (8) Chou, C.-S.; Lin, Y.-J.; Yang, R.-Y.; Liu, K.-H. Preparation of TiO₂/NiO Composite Particles and Their Applications in Dye-Sensitized Solar Cells. *Adv. Powder Technol.* **2011**, *22*, 31–42.
- (9) Nada, A. A.; Selim, H.; Bechelany, M. A Novel Photoelectrode of NiO@ZnO Nanocomposite Prepared by Pechini Method Coupled with PLD for Efficiency Enhancement in DSSCs. *Mater. Sci. Poland* **2018**, *36*, 327–336.
- (10) Wei, L.; Jiang, L.; Yuan, S.; Ren, X.; Zhao, Y.; Wang, Z.; Zhang, M.; Shi, L.; Li, D. Valence Band Edge Shifts and Charge-transfer Dynamics in Li-Doped NiO Based p-type DSSCs. *Electrochim. Acta* **2016**, *188*, 309–316.
- (11) Zhang, J.; Yu, S.-H. Carbon Dots: Large-Scale Synthesis, Sensing and Bioimaging. *Mater. Today* **2016**, *19*, 382–393.
- (12) Ye, S.-L.; Huang, J.-J.; Luo, L.; Fu, H.-J.; Sun, Y.-M.; Shen, Y.-D.; Lei, H.-T.; Xu, Z.-L. Preparation of Carbon Dots and Their Application in Food Analysis as Signal Probe. *Chin. J. Anal. Chem.* **2017**, *45*, 1571–1581.
- (13) Liu, W.; Li, C.; Ren, Y.; Sun, X.; Pan, W.; Li, Y.; Wang, J.; Wang, W. Carbon Dots: Surface Engineering and Applications. *J. Mater. Chem. B* **2016**, *4*, 5772–5788.
- (14) Xu, X.; Zhang, K.; Zhao, L.; Li, C.; Bu, W.; Shen, Y.; Gu, Z.; Chang, B.; Zheng, C.; Lin, C.; et al. Aspirin-Based Carbon Dots, a Good Biocompatibility of Material Applied for Bioimaging and Anti-Inflammation. *ACS Appl. Mater. Interfaces* **2016**, *8*, 32706–32716.
- (15) Essner, J. B.; Baker, G. A. The Emerging Roles of Carbon Dots in Solar Photovoltaics: a Critical Review. *Environ. Sci.: Nano* **2017**, *4*, 1216–1263.
- (16) Devadas, B.; Imae, T. Effect of Carbon Dots on Conducting Polymers for Energy Storage Applications. *ACS Sustainable Chem. Eng.* **2018**, *6*, 127–134.
- (17) Hu, Y.; Wang, P.; Bunker, C. E.; Teisl, L. R.; Reibold, M.; Yan, S.; Qian, H.; He, D.; Sun, Y.-P. Preparation and Optical Properties of Magnetic Carbon/Iron Oxide Hybrid Dots. *RSC Adv.* **2017**, *7*, 41304–41310.
- (18) Semeniuk, M.; Yi, Z.; Poursorkhabi, V.; Tjong, J.; Jaffer, S.; Lu, Z.-H.; Sain, M. Future Perspectives and Review on Organic Carbon Dots in Electronic Applications. *ACS Nano* **2019**, *13*, 6224–6255.
- (19) Liu, N.; Qin, Y.; Han, M.; Li, H.; Sun, Y.; Zhao, S.; Huang, H.; Liu, Y.; Kang, Z. Investigation of Regeneration Kinetics of a Carbon-Dot-Sensitized Metal Oxide Semiconductor with Scanning Electrochemical Microscopy. *ACS Appl. Energy Mater.* **2018**, *1*, 1483–1488.
- (20) Efa, M. T.; Imae, T. Effects of Carbon Dots on ZnO Nanoparticle-Based Dye-Sensitized Solar Cells. *Electrochim. Acta* **2019**, *303*, 204–210.
- (21) Varunkumar, K.; Hussain, R.; Hegde, G.; Ethiraj, A. S. Effect of Calcination Temperature on Cu Doped NiO Nanoparticles Prepared via Wet-Chemical Method: Structural, Optical and Morphological Studies. *Mater. Sci. Semicond. Process.* **2017**, *66*, 149–156.
- (22) Prasannan, A.; Imae, T. One-Pot Synthesis of Fluorescent Carbon Dots from Orange Waste Peels. *Ind. Eng. Chem. Res.* **2013**, *52*, 15673–15678.
- (23) Goel, S.; Tomar, A. K.; Sharma, R. K.; Singh, G. Highly Pseudocapacitive NiO Nanoflakes through Surfactant-Free Facile Microwave-Assisted Route. *ACS Appl. Energy Mater.* **2018**, *1*, 1540–1548.
- (24) Mishra, S.; Yogi, P.; Saxena, S. K.; Jayabalan, J.; Behera, P.; Sagdeo, P.; Kumar, R. Significant Field Emission Enhancement in Ultrathin Nano-thorn Covered NiO Nano-petals. *J. Mater. Chem. C* **2017**, *5*, 9611–9618.
- (25) El-Kemary, M.; Nagy, N.; El-Mehasseb, I. Nickel oxide Nanoparticles: Synthesis and Spectral Studies of Interactions with Glucose. *Mater. Sci. Semicond. Process.* **2013**, *16*, 1747–1752.
- (26) Rakshit, S.; Ghosh, S.; Chall, S.; Mati, S. S.; Moulik, S.; Bhattacharya, S. C. Controlled Synthesis of Spin Glass Nickel Oxide Nanoparticles and Evaluation of Their Potential Antimicrobial Activity: A Cost Effective and Eco-friendly Approach. *RSC Adv.* **2013**, *3*, 19348–19356.
- (27) Workie, Y. A.; Sabrina; Imae, T.; Krafft, M. P. Nitric Oxide Gas Delivery by Fluorinated Poly(Ethylene Glycol)/Graphene Oxide Carrier toward Pharmacotherapeutics. *ACS Biomater. Sci. Eng.* **2019**, *5*, 2926–2934.
- (28) Liu, W.; Lu, C.; Wang, X.; Liang, K.; Tay, B. K. In Situ Fabrication of Three-dimensional, Ultrathin Graphite/Carbon Nanotube/NiO Composite as Binder-free Electrode for High-Performance Energy Storage. *J. Mater. Chem. A* **2015**, *3*, 624–633.
- (29) Efa, M. T.; Imae, T. Hybridization of Carbon-Dots with ZnO Nanoparticles of Different Sizes. *J. Taiwan Inst. Chem. Eng.* **2018**, *92*, 112–117.
- (30) Wang, H.-q.; Fan, X.-p.; Zhang, X.-h.; Huang, Y.-g.; Wu, Q.; Pan, Q.-c.; Li, Q.-y. In Situ Growth of NiO Nanoparticles on Carbon Paper as a Cathode for Rechargeable Li–O₂ Batteries. *RSC Adv.* **2017**, *7*, 23328–23333.
- (31) Kim, J.-H.; Kim, T. Y.; Park, K. H.; Lee, J.-W. Electron Lifetimes in Hierarchically Structured Photoelectrodes Biotemplated from Butterfly Wings for Dye-Sensitized Solar Cells. *J. Electrochem. Int. Sci.* **2015**, *10*, 5513–5520.

- (32) Suram, S. K.; Newhouse, P. F.; Gregoire, J. M. High Throughput Light Absorber Discovery, Part 1: An Algorithm for Automated Tauc Analysis. *ACS Comb. Sci.* **2016**, *18*, 673–681.
- (33) Li, L.; Dong, T. Photoluminescence Tuning in Carbon Dots: Surface Passivation or/and Functionalization, Heteroatom Doping. *J. Mater. Chem. C* **2018**, *6*, 7944–7970.
- (34) Carolan, D.; Rocks, C.; Padmanaban, D. B.; Maguire, P.; Svrcek, V.; Mariotti, D. Environmentally Friendly Nitrogen-Doped Carbon Quantum Dots for Next Generation Solar Cells. *Sustainable Energy Fuels* **2017**, *1*, 1611–1619.
- (35) De, B.; Karak, N. A Green and Facile Approach for the Synthesis of Water Soluble Fluorescent Carbon Dots from Banana Juice. *RSC Adv.* **2013**, *3*, 8286–8290.
- (36) Sokolov, V.; Druzhinin, A.; Kim, G.; Gruzdev, N.; Yermakov, A. Y.; Uimin, M.; Byzov, I.; Shchegoleva, N.; Vykhodets, V.; Kurennykh, T. Fundamental Absorption Edge of NiO Nanocrystals. *Phys. B* **2013**, *430*, 1–5.
- (37) Adhikary, J.; Chakraborty, P.; Das, B.; Datta, A.; Dash, S. K.; Roy, S.; Chen, J.-W.; Chattopadhyay, T. Preparation and Characterization of Ferromagnetic Nickel Oxide Nanoparticles from three Different Precursors: Application in Drug Delivery. *RSC Adv.* **2015**, *5*, 35917–35928.
- (38) Liu, L.; Mi, Z.; Hu, Q.; Li, C.; Li, X.; Feng, F. Green Synthesis of Fluorescent Carbon Dots as an Effective Fluorescence Probe for Morin Detection. *Anal. Methods* **2019**, *11*, 353–358.
- (39) Zhang, Y.-Q.; Ma, D.-K.; Zhang, Y.-G.; Chen, W.; Huang, S.-M. N-Doped Carbon Quantum Dots for TiO₂-Based Photocatalysts and Dye-Sensitized Solar Cells. *Nano Energy* **2013**, *2*, 545–552.
- (40) Zhu, W.; Zhao, Y.; Duan, J.; Duan, Y.; Tang, Q.; He, B. Carbon Quantum Dot Tailored Counter Electrode for 7.01%-rear Efficiency in a Bifacial Dye-Sensitized Solar Cell. *Chem. Commun.* **2017**, *53*, 9894–9897.
- (41) Choi, Y.; Choi, Y.; Kwon, O. H.; Kim, B. S. Carbon Dots: Bottom-Up Syntheses, Properties, and Light-Harvesting Applications. *Chem. - Asian J.* **2018**, *13*, 586–598.
- (42) Alemu, G.; Li, J.; Cui, J.; Xu, X.; Zhang, B.; Cao, K.; Shen, Y.; Cheng, Y.; Wang, M. Investigation on Regeneration Kinetics at Perovskite/Oxide Interface with Scanning Electrochemical Microscopy. *J. Mater. Chem. A* **2015**, *3*, 9216–9222.
- (43) Barman, M. K.; Mitra, P.; Bera, R.; Das, S.; Pramanik, A.; Parta, A. An Efficient Charge Separation and Photocurrent Generation in the Carbon Dot–Zinc Oxide Nanoparticle Composite. *Nanoscale* **2017**, *9*, 6791–6799.
- (44) Nikolaou, V.; Charisiadis, A.; Charalambidis, G.; Coutsolelos, A. G.; Odobel, F. Recent Advances and Insights in Dye-Sensitized NiO Photocathodes for Photovoltaic Devices. *J. Mater. Chem. A* **2017**, *5*, 21077–21113.
- (45) Yang, X.; Yanagida, M.; Han, L. Reliable Evaluation of Dye-Sensitized Solar Cells. *Energy Environ. Sci.* **2013**, *6*, 54–66.
- (46) Liu, Y.; Wang, J. Co-Sensitization of TiO₂ by PbS Quantum Dots and Dye N719 in Dye-Sensitized Solar Cells. *Thin Solid Films* **2010**, *518*, e54–e56.
- (47) Hirose, F.; Shikaku, M.; Kimura, Y.; Niwano, M. IR Study on N719 Dye Adsorption with High Temperature Dye Solution for Highly Efficient Dye-Sensitized Solar Cells. *J. Electrochem. Soc.* **2010**, *157*, B1578–B1581.
- (48) Cai, C.-Y.; Tseng, S.-K.; Kuo, M.; Lin, K.-Y. A.; Yang, H.; Lee, R.-H. Photovoltaic Performance of a N719 Dye Based Dye-Sensitized Solar Cell with Transparent Macroporous Anti-ultraviolet Photonic Crystal Coatings. *RSC Adv.* **2015**, *5*, 102803–102810.
- (49) Honda, M.; Yanagida, M.; Han, L.; Miyano, M. X-ray Characterization of Dye Adsorption in Coadsorbed Dye-Sensitized Solar Cells. *J. Phys. Chem. C* **2013**, *117*, 17033–17038.
- (50) Wen, P.; Han, Y.; Zhao, W. Influence of TiO₂ Nanocrystals Fabricating Dye-Sensitized Solar Cell on the Absorption Spectra of N719 Sensitizer. *Int. J. Photoenergy* **2012**, *2012*, No. 906198.
- (51) Qin, P.; Zhu, H.; Edvinsson, T.; Boschloo, G.; Hagfeldt, A.; Sun, L. Design of an Organic Chromophore for P-Type Dye-Sensitized Solar Cells. *J. Am. Chem. Soc.* **2008**, *130*, 8570–8571.
- (52) Dutta, M.; Sarkar, S.; Ghosh, T.; Basak, D. ZnO/Graphene Quantum Dot Solid-State Solar Cell. *J. Phys. Chem. C* **2012**, *116*, 20127–20131.
- (53) Sun, M.; Qu, S.; Ji, W.; Jing, P.; Li, D.; Qin, L.; Cao, J.; Zhang, H.; Zhao, J.; Shen, D. Towards Efficient Photoinduced Charge Separation in Carbon Nano Dots and TiO₂ Composites in Visible Region. *Phys. Chem. Chem. Phys.* **2015**, *17*, 7966–7971.
- (54) Pan, J.; Sheng, Y.; Zhang, J.; Huang, P.; Zhang, X.; Feng, B. Photovoltaic Conversion Enhancement of a Carbon Quantum Dots/p-Type CuAlO₂/n-Type ZnO Photoelectric Device. *ACS Appl. Mater. Interfaces* **2015**, *7*, 7878–7883.
- (55) Kokal, R. K.; Kumar, P. N.; Deepa, M.; Srivastava, A. K. Lead selenide Quantum Dots and Carbon Dots Amplify Solar Conversion Capability of a TiO₂/CdS Photoanode. *J. Mater. Chem. A* **2015**, *3*, 20715–20726.
- (56) Zhao, Y.; Duan, J.; He, B.; Jiao, Z.; Tang, Q. Improved Charge Extraction with N-Doped Carbon Quantum Dots in Dye-Sensitized Solar Cells. *Electrochim. Acta* **2018**, *282*, 255–262.
- (57) Bora, A.; Mohan, K.; Dolui, S. K. Carbon Dots as Co-sensitizers in Dye Sensitized Solar Cell and Fluorescence Chemosensor for 2,4,6-Trinitrophenol Detection. *Ind. Eng. Chem. Res.* **2019**, *58*, 22771–22778.
- (58) Liu, L.; Yu, X.; Yi, Z.; Chi, F.; Wang, H.; Yuan, Y.; Li, D.; Xu, K.; Zhang, X. High Efficiency Solar Cells Tailored Using Biomass-Converted Graded Carbon Quantum Dots. *Nanoscale* **2019**, *11*, 15083–15090.
- (59) Gao, N.; Huang, L.; Li, T.; Song, J.; Hu, H.; Liu, Y.; Ramakrishna, S. Application of Carbon Dots in Dye-Sensitized Solar Cells: A review. *J. Appl. Polym. Sci.* **2020**, *137*, No. 48443.
- (60) Pan, J.; Sheng, Y.; Zhang, J.; Huang, P.; Zhang, X.; Feng, B. Photovoltaic Conversion Enhancement of a Carbon Quantum Dots/p-Type CuAlO₂/n-Type ZnO Photoelectric Device. *ACS Appl. Mater. Interfaces* **2015**, *7*, 7878–7883.